Adapted Anisotropic Gaussian SIFT Matching Strategy for SAR Registration

Feng Wang, Hongjian You, and Xingyu Fu

***Abstract*—In this letter, we propose an adapted anisotropic Gaussian scale-invariant feature transform (AAG-SIFT) method to find feature matches for synthetic aperture radar (SAR) image registration. First, features are detected and described in an AAG scale space. The scale space is built adaptively to local structures. Noises are blurred, but details and edges remain unaffected in this scale space. Compared with traditional SIFT-based matching methods, features extracted by AAG-SIFT are more stable and precise. Then, the dominant orientation consistency (DOC) property is analyzed and adopted to improve the matching stability. The correct matching rate is significantly increased by DOC matching. Experiments on various SAR images demonstrate the applicability of AAG-SIFT to find stable and precise feature matches for SAR registration.**

***Index Terms*—Anisotropic Gaussian scale space, synthetic aperture radar (SAR) image registration, scale-invariant feature transform (SIFT).**

I. Introduction

SYNTHETIC aperture radar (SAR) image registration is a key step in many applications, such as image fusion, image mosaic, change detection, and so on. Image registration methods can be divided into two categories: intensity-based methods and feature-based methods. Compared with intensity-based methods, feature-based methods depending on matching distinctive features have higher precision and effectiveness.

Among feature-based methods, scale-invariant feature transform (SIFT)-based methods garner more and more attention in the remote sensing fields, owing to their excellent performance [1]–[4]. Although progress has been reported in adapting SIFT approaches for SAR image registration, there is still some room for improvement. It is a challenging task to find matches between SAR images due to the differences in gray information caused by local geometric deformations and speckle.

Traditional SIFT features are detected and described in Gaussian scale space. The Gaussian kernel is the simplest option, but not the only one, to build a scale-space representation. It suffers from some drawbacks. First, Gaussian blurring does not respect natural boundaries of objects. Both details and noises are smoothed to the same degree. This results in a reduction in localization accuracy [5]. Second, Gaussian scale space cannot adapt to any shape other than round. The Gaussian scale space implementation considers only round blob features. However, objects in the real world have other shapes with different spatial orientations.

Manuscript received April 28, 2014; accepted June 2, 2014. Date of publication July 2, 2014; date of current version August 14, 2014.

The authors are with the Key Laboratory of Technology in Geo-spatial Information Processing and Application System, Institute of Electronics, Chinese Academy of Sciences, Beijing 100190, China (e-mail: wfeng_gucas@126.com).

Color versions of one or more of the figures in this paper are available online at http://ieeexplore.ieee.org.

Digital Object Identifier 10.1109/LGRS.2014.2330593

Many anisotropic scale-space approaches have been introduced to solve the aforementioned problems. Perona and Malik [6] analyzed anisotropic scale-space representation realized using nonlinear diffusion formulation. Alcantarilla *et al.* [5] introduced KAZE features that detect and describe features in nonlinear scale space built using additive-operator-splitting techniques. It exhibited good performance for traditional image matching applications. Wang *et al.* [3] proposed BFSIFT, whose scale space is built using a bilateral filter, to improve the applicability of finding feature matches for SAR images. Gobara and Suter [7] and Skoch and Gauch [8] detected features using anisotropic Gaussian diffusion based on image derivative and Sobel gradient, respectively. These methods preserve edges better than the traditional SIFT-based methods. However, they did not consider the influence of noises. Noises, particularly these around edges, impair the performance of these matching methods.

In this letter, we propose an adapted anisotropic Gaussian (AAG) SIFT (AAG-SIFT) matching scheme to obtain stable and precise matches for SAR registration. First, an AAG filter is introduced to construct an AAG scale space for feature detection and description. The AAG filter is built adaptively based on local structures represented by a second-moment matrix. It is robust to noises and can preserve more details than the Gaussian filter. Second, a dominant orientation consistency (DOC) matching method is used to refine matches based on the descriptor distance and DOC criterion. The correct matching rate (CMT) is significantly increased by using the DOC matching method. Finally, matches are obtained by random sample consensus (RANSAC) to estimate transformation parameters used in image registration [9]. Experiments on simulated and various SAR images demonstrate the ability of AAG-SIFT to find stable and precise matches for SAR registration.

II. Proposed Method

SIFT consists of three major stages. First, Gaussian scale space is constructed by convolving the image with Gaussian filters at different scales. A series of Difference of Gaussian (DoG) images are obtained by subtracting the adjacent Gaussian images. Extrema of the DOG images are detected as keypoints. Second, dominant orientation is calculated for each keypoint. The descriptor of each keypoint is constructed based on the gradients in the local image patches aligned by its dominant orientation. Finally, feature points are matched using the nearest neighbor distance ratio (NNDR). More details about SIFT can be found in [2].

When SIFT is applied to SAR registration, speckle deteriorates the process of feature detection and causes many unrepeatable keypoints. Most of these unrepeatable keypoints are detected in the first octave [1], [3]. Therefore, features are detected starting from the second octave in our proposed method.

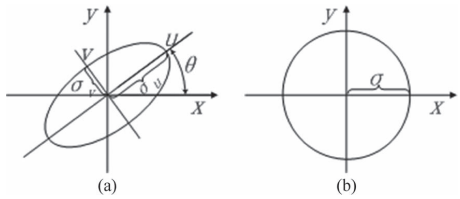

Fig. 1. (a) Anisotropic Gaussian with aspect ratio of 1:2 and orientation $\theta = \pi/4$. (b) Isotropic Gaussian.

A. AAG Scale-Space SIFT

KAZE and BFSIFT can overcome the drawbacks of Gaussian scale space based on nonlinear diffusion formulation [6]. However, nonlinear diffusion formulation detects edges based on image gradient and would not smooth images in edge regions. Hence, they are sensitive to noises particularly around edges. We propose to build an AAG scale space by replacing the Gaussian filter with a modified AAG filter based on local statistical characteristics. Features are then detected and described in this AAG scale space using the same procedures of SIFT [2].

The AAG filter is constructed based on the strategy that edge areas are smoothed by oriented and sharped elliptical Gaussian masks, whereas homogeneous regions are smoothed by radial masks. It preserves edges better than the Gaussian filter and is more robust to noises than nonlinear diffusion formulation. The general case of an oriented anisotropic Gaussian filter [see Fig. 1(a)] in two dimensions is defined as follows [10]:

$$g_\theta(u, v; \sigma_u, \sigma_v, \theta) = \frac{1}{\sqrt{2\pi}\sigma_u} \exp\left\{-\frac{1}{2}\frac{u^2}{\sigma_u^2}\right\} * \frac{1}{\sqrt{2\pi}\sigma_v} \exp\left\{-\frac{1}{2}\frac{v^2}{\sigma_v^2}\right\} \quad (1)$$

where "$*$" denotes convolution; θ indicates the orientation of the filter; σ_u and σ_v denote scaling parameters in the u-axis and v-axis, with the u-axis being in the direction of θ, the v-axis being orthogonal to θ, and

$$\begin{pmatrix} u \\ v \end{pmatrix} = \begin{bmatrix} \cos\theta & \sin\theta \\ -\sin\theta & \cos\theta \end{bmatrix} \begin{pmatrix} x \\ y \end{pmatrix}. \quad (2)$$

Compared with isotropic Gaussian filters, anisotropic Gaussian filters add a spatial orientation θ and two scale parameters σ_u, σ_v (see Fig. 1). Thus, it can fit the local structures better.

The first step to construct the AAG filter is to get the orientation θ corresponding to the edge direction. An orientation histogram is formed from the gradient orientations of the sample points around the current point. Each sample added to the histogram is weighted by its gradient magnitude and by a Gaussian-weighted circular window. The interference of noise is reduced by doing this. The highest peak in the orientation histogram is regarded as the gradient direction of the local region. The orientation θ of the AAG filter corresponds to the direction orthogonal to the local gradient direction.

The second step is to fix the shape of the ellipse. We set the scaling parameter σ_u of octave o and sublevel s the same as $\sigma(o, s)$ defined in Gaussian scale space, as follows:

$$\sigma_u = \sigma(o, s) = \sigma_0 2^{\frac{(o+s)}{S}},\ o \in [0, \ldots, O-1],\ s \in [0, \ldots, S-1] \quad (3)$$

where σ_o is the base scale level; O and S are the numbers of octaves and sublevels of the scale space, respectively; o and s indicate the octave and sublevel indexes, respectively. The value of σ_v is determined by a second-moment matrix, which is often used to adapt the shape of a region to local image structures [11], [12]. The second-moment matrix M at scale of σ around point $P(x_0, y_0)$ is defined as follows:

$$M(P, \sigma) = \sum_{x,y} w_\sigma(x, y) \begin{bmatrix} I_x^2(x, y) & I_x I_y(x, y) \\ I_x I_y(x, y) & I_y^2(x, y) \end{bmatrix} \quad (4)$$

where I_x and I_y are the respective derivatives in the x- and y-directions at point (x, y); σ corresponds to the current scale $\sigma(o, s)$, in which the filter is used to blur. The weighting function $w_\sigma(x, y)$ is an isotropic circular Gaussian (4), as follows:

$$w_\sigma(x, y) = g(x, y, \sigma) = \frac{1}{2\pi\sigma^2} e^{\left(-\frac{x^2+y^2}{2\sigma^2}\right)}. \quad (5)$$

The eigenvalues of the second-moment matrix characterize the curvature and shape of the local pixel intensities. There are three cases to be considered [11]:

a) One eigenvalue is large and the other is small: edge region;
b) Both eigenvalues are small: flat region;
c) Both eigenvalues are large: corner region.

A measure of the isotropy describing the statistical characteristics around a local region is defined as follows [12]:

$$\gamma = \frac{\lambda_{\min}(M)}{\lambda_{\max}(M)} \quad (6)$$

where $\lambda_{\max}(M)$ denotes the larger eigenvalue, and $\lambda_{\min}(M)$ denotes the smaller eigenvalue. The shape of the AAG filter is defined based on isotropy measure as follows:

$$\sigma_v = \sigma_u^* \gamma^n. \quad (7)$$

We recommend exponent n being 1/3, which was empirically obtained after various experiments. Using this method, the edge regions (case A) are filtered by a directional elliptical Gaussian filter, while flat and corner regions (cases B and C) are filtered by isotropic circular Gaussian.

The filtered results of Gaussian smoothing and anisotropic Gaussian smoothing are shown in Fig. 2. Compared with the Gaussian blurred image, the edges of the anisotropic Gaussian

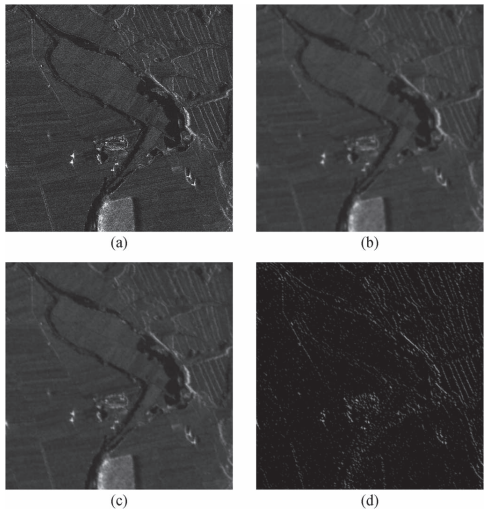

Fig. 2. (a) Original SAR image. (b) Image filtered by five passes of isotropic Gaussian with $\sigma = 2$. (c) Image filtered by five passes of anisotropic Gaussian with $\sigma_u = 2$. (d) Difference image of (b) and (c).

blurred image remain sharp, while flat areas are nearly blurred to the same degree. The result of using anisotropic Gaussian smoothing is impressive, particularly after several iterations of blurring. Although nonedge areas are blurred, edges remain sharp and crisp. The AAG scale space is expected to preserve details of SAR images and extract stable features.

B. DOC Matching

The distinctiveness of feature descriptors for SAR images is impaired because SAR images contain less texture details than optical images. Furthermore, there are many similar patterns in typical SAR images. Outliers caused by these similar patterns could not be removed by descriptor-based matching methods, such as NNDR matching [2] and dual matching (DM) [3]. Li *et al.* [4] introduced scale-orientation joint restriction criteria to remove outliers for remote sensing images with notable differences from different spectra or different sensors. However, it is not suitable to match two SAR images with similar patterns. Motivated by Li's method, we propose a DOC matching method to refine matches based on DOC property.

Considering two SAR images I_1 and I_2 with similarity transformation of scaling s, rotation a, and translation (t_x, t_y), the relation between them is given by

$$\begin{bmatrix} u \\ v \end{bmatrix} = \begin{bmatrix} s\cos a & -s\sin a \\ s\sin a & s\cos a \end{bmatrix} \begin{bmatrix} x \\ y \end{bmatrix} + \begin{bmatrix} t_x \\ t_y \end{bmatrix} \tag{8}$$

where (x, y) and (u, v) indicate the corresponding points.

The angle θ of two points (x_1, y_1) and (x_2, y_2) in I_1 is given by

$$\theta = \arctan\left(\frac{y_1 - y_2}{x_1 - x_2}\right). \tag{9}$$

The angle ϕ of the corresponding two points (u_1, v_1) and (u_2, v_2) in I_2 is given by

$$\phi = \arctan\left(\frac{v_1 - v_2}{u_1 - u_2}\right) = a + \theta \tag{10}$$

where a indicates the rotation of the two images. It can be concluded that the corresponding subregions rotate the same degrees as the original two images do. Therefore, the dominant orientations of the corresponding features are consistent. In most application cases, geometric distortions found in remotely sensed images can be modeled by similarity transformation without large errors [4]. Thus, DOC property is used to refine matches. The DOC matching is carried out as follows.

Step 1) Descriptor-based matching, such as DM, is conducted to obtain an initial set of feature matches.

Step 2) An orientation histogram is formed from the dominant orientation deflections of the initial matches to get the deflection of the two images. The dominant orientation deflection $\delta_{i,j}$ of two features F_i and F'_j is formulated as

$$\delta_{i,j} = \pi - \left|\pi - \left|\theta(F_i) - \theta\left(F'_j\right)\right|\right|,\ \theta(F_i),\ \theta\left(F'_j\right) \in (-\pi, \pi] \tag{11}$$

where $\theta(F_i)$ and $\theta(F'_j)$ are the dominant orientations of F_i and F'_j. $|\cdot|$ denotes the absolute value. The deflection δ of these two images is the orientation corresponding to the greatest bin value in the orientation histogram.

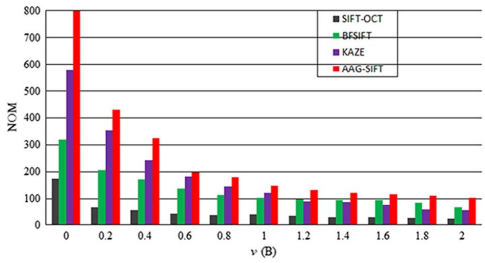

Fig. 3. NOMs of the four tested methods on simulated images with speckle noise.

Step 3) Outliers are removed from the initial matching set by the DOC criterion defined as follows:

$$\delta - \pi/N \le \delta_{i,j} \le \delta + \pi/N \tag{12}$$

where N indicates the number of bins in the orientation histogram. We only accept matches fitting with the DOC criterion.

III. Experiments and Results

Experiments were carried out to validate the effectiveness of AAG-SIFT. Diverse data sets were tested, including simulated images and georectified SAR images taken at different times, from different look angles, and from different orbit directions. The proposed method is compared with not only SIFT-OCT [1] and BFSIFT [3] designed for SAR registration but also KAZE [5], whose main modification is based on nonlinear scale space. Although KAZE was not designed for SAR images, it performs very well for traditional image matching applications. The evaluation has been carried out using the following criteria.

1) Number of correct matches (NOM): Matches refined by RANSAC are used to calculate the registration parameters. These matches are regarded as correct matches.
2) CMT: The ratio of NOM to the number of matches before RANSAC is calculated to examine the performance of DOC. If the CMT value is too small, RANSAC will conduct numerous iterations and may even not be able to obtain the correct matches. Larger CMT indicates that it is more likely to get correct matching.
3) Root-mean-square error (RMSE): RMSE is computed to judge the alignment accuracy. For each time to calculate RMSE, thirty test-point (TP) pairs are selected manually. From these manually selected TPs, 20 pairs are used to calculate the transformation model, and the remaining ten pairs are used to calculate the manual RMSE. Given two-point sets, which are manually selected or obtained by the tested methods, their RMSE is calculated as follows:

$$\text{RMSE} = \left(\sum_{i=1}^{m} \frac{1}{m}\left[(uX_i + vY_i + \Delta X - X'_i)^2 + (uY_i - vX_i + \Delta Y - Y'_i)^2\right]\right)^{\frac{1}{2}} \tag{13}$$

where (X_i, Y_i) and (X'_i, Y'_i) are the coordinates of the ith point pair; m denotes the number of the point pairs. The vector $(u, v, \Delta X, \Delta Y)$ denotes the parameters of the transformation model. For each test case, the algorithm is executed five times to suppress the instability caused by manually selected TP pairs. In addition, their average is computed as the final RMSE [4].

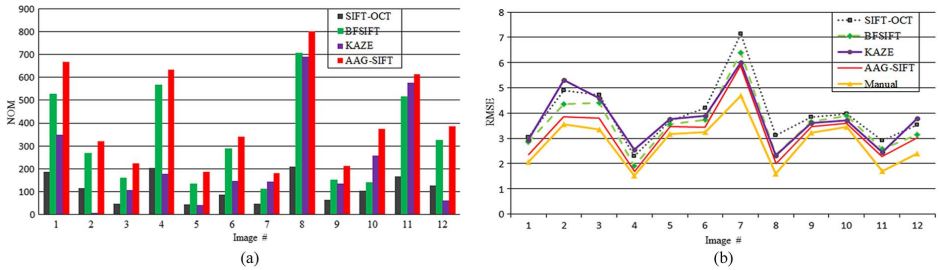

Fig. 4. Experimental results of the four matching methods on airborne images from different look angles: (a) NOMs; (b) RMSEs.

TABLE I
CMTs OF AAG-SIFT WITH NNDR MATCHING OR DOC MATCHING

Image#	1	2	3	4	5	6	7	8	9	10
NNDR	0.86	0.76	0.69	0.88	0.85	0.83	0.48	0.83	0.76	0.83
DOC	0.94	0.88	0.88	0.95	0.93	0.92	0.57	0.95	0.83	0.91

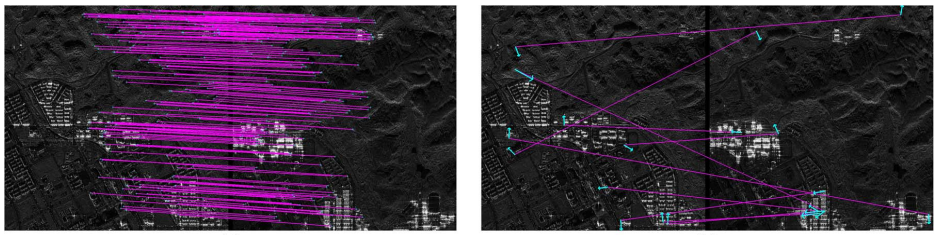

Fig. 5. Matching experiment on spaceborne images acquired from different look angles. The look angles of the left and right images are about 43° and 49°, respectively: (a) matches found by AAG-SIFT; (b) outliers filtered out by DOC. The arrows indicate the dominant orientation.

A. *Experiment on Simulated Images With Speckle Noise*

Here, the four matching methods are carried out on simulated images with different speckle. We add multiplicative noise to the Lena image I using the equation $IB = B^*I$. B denotes a Gaussian white noise with mean $E(B) = 1$ and variance $v(B) = 0, 0.2, 0.4, \ldots, 2$. The four matching methods are used to find matches between the original image I and the noised image IB. The experimental results are shown in Fig. 3. The NOMs of the four matching methods decrease rapidly with the influence of speckle. This indicates that it is difficult to register SAR images with much speckle. AAG-SIFT performs the best for reducing the influence of speckle noise. It can always find the most matches of the four matching methods.

B. *Experiment on Airborne Images From Different Look Angles*

Twelve pairs of airborne X-band images, with a resolution of 0.5 m, from different look angles are tested. These images were acquired on December 4 and 7, 2010, over Changzhi, China.

Comparing the results shown in Fig. 4, AAG-SIFT can always find the most matches. It has the best performance in obtaining correct matches of the four matching methods. The performance of KAZE is unstable. It may get comparable matches with AAG-SIFT, but only gets few in other cases. Moreover, the alignment accuracy of the proposed method is the highest and is close to the baseline standard computed using manually selected TP pairs. The RMSEs are smaller when NOMs are larger. This phenomenon indicates that more matches are desirable for calculating registration parameters.

The CMTs of AAG-SIFT using NNDR matching [11] or DOC matching are provided in Table I. The CMTs are increased by DOC matching. This can be explained in Fig. 5. The outliers filtered out by DOC are shown in Fig. 5(b). The regions around the corresponding mismatches are similar. These mismatches have similar descriptors and cannot be removed by descriptor-based methods. However, their dominant orientation deflections are different with the rotation of the two images. Thus, they are filtered out by DOC matching.

C. *Experiment on Spaceborne Images at Different Times and Orbit Directions*

We chose 20 pairs of TerraSAR-X spaceborne SAR images in this part. The first ten pairs of images were taken at different times, whereas the other ten pairs were from different orbit directions.

The NOMs and RMSEs of the four matching methods are shown in Fig. 6. Among the 20 pairs of images, 18 pairs are matched by AAG-SIFT and BFSIFT, while 6 and 12 pairs are matched by SIFT-OCT and KAZE. This indicates that AAG-SIFT and BFSIFT are more stable than the other two matching methods. For the 18 pairs of aligned images, since the AAG filter is less sensitive to noises than the bilateral filter, AAG-SIFT yields better results than BFSIFT, in terms of correct matching number and alignment accuracy.

The AAG-SIFT matching results of two images acquired from different orbit directions are presented in Fig. 7. It is a challenging problem to match these two images with much speckle and significant differences in the appearance of the same scene. However, the ridges of buildings and rivers, which are represented as edge features, are stable regardless of noises and distortions. The AAG scale space is robust to noises and can preserve these stable details unaffected. Therefore, AAG-SIFT is able to find stable and robust feature matches. Fig. 7(a) shows that the feature matches distribute mainly around edge

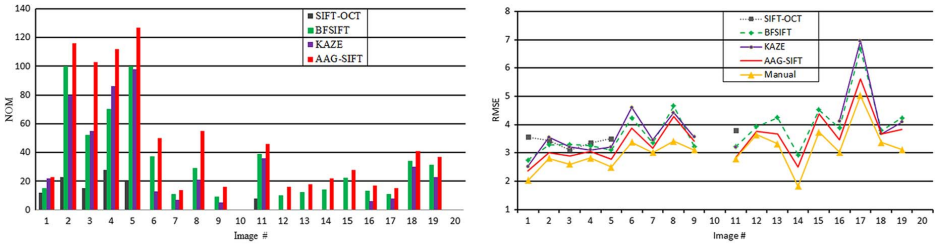

Fig. 6. Experimental results of the four matching methods on spaceborne images. The first ten images are acquired at different times, and the last ten images are from different orbit directions: (a) NOMs; (b) RMSEs.

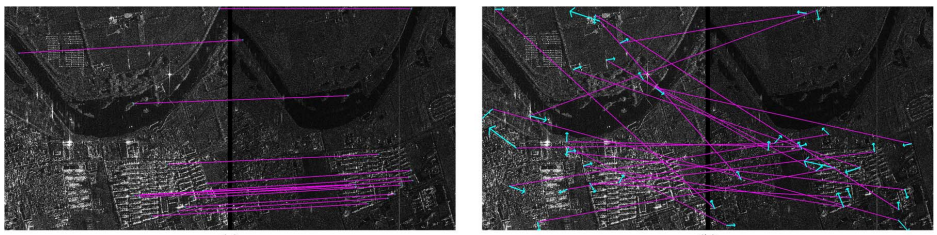

Fig. 7. Matching experiment on spaceborne images from different orbit directions. The left image is acquired in ascending orbit, while the right is in descending orbit. (a) Matches found by AAG-SIFT and (b) outliers filtered by DOC. The arrows indicate the main orientation.

TABLE II
CMTs OF AAG-SIFT WITH NNDR OR DOC MATCHING

Image #	1	2	3	4	5	6	7	8	9	10	11	12	13	14	15	16	17	18	19	20
NNDR	0.51	0.81	0.76	0.72	0.69	0.86	0.25	0.74	0.42	-	0.64	0.19	0.36	0.45	0.58	0.35	0.33	0.60	0.69	-
DOC	0.92	0.86	0.87	0.82	0.77	0.89	0.43	0.83	0.68	-	0.79	0.32	0.42	0.72	0.69	0.54	0.56	0.90	0.82	-

TABLE III
AVERAGE RUNNING TIME OF THE FOUR MATCHING METHODS

Method	SIFT-OCT	BFSIFT	KAZE	AAG-SIFT
Time (s)	1.0	8.5	10.3	10.2

areas. Fig. 7(b) shows the outliers removed by DOC matching. There are many similar regions in these two SAR images. They cause many outliers, which cannot be removed by descriptor-based matching methods. However, DOC matching can filter them out, depending on their dominant orientation deflections.

The CMTs of the 18 aligned images are listed in Table II. The CMTs are markedly increased by DOC matching. This makes it easier to estimate a reasonable model and obtain the correct matches.

The average running time of the tested methods are shown in Table III. AAG-SIFT is computationally more expensive than SIFT-OCT, but comparable to BFSIFT and KAZE. This is mainly due to the computation of an anisotropic scale space. We are concentrating on how to calculate AAG-SIFT faster without compromising its performance. Many associated methods, such as the one proposed in [12], may be employed to accelerate the construction of AAG-SIFT.

IV. CONCLUSION

This letter presents a feature-based matching approach to find matches for SAR registration. AAG is introduced to build image scale space without impairing the edge information and fine details. Features detected and described in this anisotropic scale space are stable and accurate. DOC property is analyzed and used to filter out mismatches with similar descriptors. The DOC matching strategy can significantly increase the CMT. Experiments are carried out with simulated images and SAR images at different times, from different look angles, and from different orbit directions. The results demonstrate the applicability of AAG-SIFT to find stable and precise matches for SAR image registration.

REFERENCES

[1] P. Schwind, S. Suri, P. Reinartz, and A. Siebert, "Applicability of the SIFT operator to geometric SAR image registration," *Int. J. Remote Sens.*, vol. 31, no. 8, pp. 1959–1980, Mar. 2010.
[2] D. G. Lowe, "Distinctive image features from scale-invariant keypoints," *Int. J. Comput. Vis.*, vol. 60, no. 2, pp. 91–110, Nov. 2004.
[3] S. Wang, H. You, and K. Fu, "BFSIFT: A novel method to find feature matches for SAR image registration," *IEEE Geosci. Remote Sens. Lett.*, vol. 9, no. 4, pp. 649–653, Jul. 2012.
[4] Q. Li, G. Wang, J. Liu, and S. Chen, "Robust scale-invariant feature matching for remote sensing image registration," *IEEE. Geosci. Remote Sens Lett.*, vol. 6, no. 2, pp. 287–291, Apr. 2009.
[5] P. F. Alcantarilla, A. Bartoli, and A. J. Davison, "KAZE features," in *Conf. Rec. IEEE IAS Annu. Meeting*, 2012, pp. 214–227.
[6] P. Perona and J. Malik, "Scale space and edge detection using anisotropic diffusion," *IEEE Trans. Pattern Anal. Mach. Intell.*, vol. 12, no. 7, pp. 629–637, Jul. 1990.
[7] M. Gobara and D. Suter, "Feature detection with an improved anisotropic filter," in *Asian Conf. Comput. Vis.*, Hyderabad, India, 2006, pp. 643–652.
[8] W. Skoch and J. Gauch, "The effects of anisotropic Gaussian diffusion in scale invariant feature detection," in *Proc. IEEE ICSIPA*, Kuala Lumpur, Malaysia, 2011, pp. 524–529.
[9] M. A. Fischler and R. C. Bolles, "Random sample consensus: A paradigm for model fitting with applications to image analysis and automated cartography," *Commun. ACM*, vol. 24, no. 6, pp. 381–395, Jun. 1981.
[10] J. M. Geusebroek, A. W. Smeulders, and J. Van De Weijer, "Fast anisotropic Gauss filtering," *IEEE Trans. Image Process.*, vol. 12, no. 8, pp. 938–943, Aug. 2003.
[11] C. Harris and M. Stephens, "A combined corner and edge detector," in *Proc. 4th Alvey Vis. Conf.*, Manchester, U.K., 1988, pp. 147–151.
[12] K. Mikolajczyk and C. Schmid, "Scale & affine invariant interest point detectors," *Int. J. Comput. Vis.*, vol. 60, no. 1, pp. 63–86, Nov. 2004.